

# INTERPOLATION OF TURBULENT MAGNETIC FIELDS AND ITS CONSEQUENCES ON DIFFUSIVE COSMIC RAY PROPAGATION

L. Schlegel,<sup>1</sup> A. Frie,<sup>1</sup> B. Eichmann,<sup>1</sup> P. Reichherzer,<sup>1</sup> and J. Becker Tjus<sup>1</sup>

<sup>1</sup>*Ruhr Astroparticle and Plasma Physics Center (RAPP Center), Ruhr-Universität Bochum, Institut für Theoretische Physik IV/  
Plasma-Astroteilchenphysik, 44780 Bochum, Germany*

## Abstract

Numerical simulations of the propagation of charged particles through magnetic fields solving the equation of motion often leads to the usage of an interpolation in case of discretely defined magnetic fields, typically given on a homogeneous grid structure. However, the interpolation method influences the magnetic field properties on the scales of the grid spacing and the choice of interpolation routine can therefore change the result. At the same time, it provides an impact, i.e. error, on the spatial particle distribution.

We compare three different interpolation routines – trilinear, tricubic and nearest neighbor interpolation – in the case of turbulent magnetic fields and show that there is no benefit in using trilinear interpolation. We show that in comparison, the nearest neighbor interpolation provides the best performance, i.e. requires least CPU time and results in the smallest error. In addition, we optimize the performance of an algorithm that generates a continuous grid-less turbulent magnetic field by more than an order of magnitude. This continuous method becomes practicable for the simulation of large particle numbers and its accuracy is only limited by the used number of wavemodes. We show that by using more than 100 wavemodes the diffusive behavior of the spatial particle distribution in form of the diffusion coefficient is determined with an error less than a few percentage.

## INTRODUCTION

Turbulent magnetic fields are present in almost every astrophysical environment and so they yield a key impact on the properties of cosmic rays (CRs)<sup>1</sup> that penetrate the Earth's atmosphere. First, these fields play a crucial role at the cosmic accelerators in order to isotropize the particle distribution and afterwards, during the propagation to Earth, turbulent magnetic fields often provide the dominant magnetic field, especially in the large-scale structure of the Universe, e.g. in the filaments and sheets. And even in the case of the Galactic magnetic field, the random magnetic field component provides a significant contribution (Beck et al. 2016). Thus, the identification of the CR sources is strongly coupled to the understanding of the turbulent magnetic fields. But in particular the extragalactic magnetic fields (EGMFs) are hardly constrained by observations. Their filling factors, which provide the fraction of the total volume filled with magnetic fields higher than a certain reference value, vary between different models by several orders of magnitude (Alves Batista et al. 2017). Another source of uncertainty that is usually not taken into account, results from the inevitable interpolation of a magnetic field that is discretely defined on a grid. Usually the grid provides a homogeneous structure, defined by a certain number  $n$  of grid points on each of which the information on the magnetic field is provided, as well as the spacing  $d$  between them. Obviously, such a grid structure is unable to cover small-scale variations of the field accurately, e.g. the impact of single galaxies and galaxy clusters on the total EGMF structure, due to limited memory space. To a certain extent this issue can be solved by using a multi-resolution grid (Müller 2016), but the main problem of the interpolation remains. So, even in the case of large-scale variations of the vector field, e.g. the turbulent magnetic field structure of the voids, filaments and sheets, the interpolation method always provides an interpolation error depending on the chosen method and the grid resolution, in particular. In the case of vectorial data on the grid point, either a component-wise interpolation or an interpolation that separates the direction and the magnitude can be performed. Moreover, also a combination of both is possible, e.g. interpolate component-wise at first and change the magnitude to the mean length of the surrounding vectors through normalization afterwards. In

<sup>1</sup> CRs are composed of ionized nuclei (predominantly protons) with energies above a few GeV.

principle, all of these procedures either struggle with the conservation of the mean of the magnitudes given on the grid points or the uniqueness of the interpolated direction.

A commonly used, fast routine is the *trilinear* interpolation, hereafter abbreviated as TL. It is defined via the discretization of the to-be interpolated function (that in principle can be either scalar or vectorial as in our case)  $f(x, y, z)$

$$f(x, y, z) = \sum_{i,j,k=0}^1 f(i, j, k) x^i y^j z^k (1-x)^{i+1} (1-y)^{j+1} (1-z)^{k+1} \quad (1)$$

in three dimensions in a unit cube. Here, the coordinates  $x, y, z$  in the cube volume denote the position where an approximation of the grid data is calculated. In the case of vectorial data, like magnetic fields, typically each component at the coordinates is treated separately referring to the component-wise interpolation approach. However, this interpolation method systematically yields a lower magnetic field strength between the grid points than at the grid points. Thus, CRs typically show deflections that are expected to be systematically smaller than expected. But also the direction-magnitude separated TL routine keeps the extreme values at the grid points, like in the case of scalar fields, and generates structural artifacts as illustrated in Fig. 3a. In addition, the TL does not keep the magnetic field divergence free.

A routine that includes more information on the given data at the grid points is the *tricubic* interpolation, hereafter abbreviated as TC, which is given by Lekien & J. E. (2005):

$$f(x, y, z) = \sum_{i,j,k=0}^N a_{ijk} x^i y^j z^k. \quad (2)$$

There are different possibilities of how to determine the necessary constraints resulting in the coefficients  $a_{ijk}$  gaining different properties of the interpolant (see Lekien & J. E. (2005)). We focus on the restriction that the derivative at a certain point is given by the difference quotient of the previous and following grid point defined as  $\tau(p_{i+1} - p_{i-1})$ , leading to the so called Catmull-Rom-Spline-Interpolation with a tension-parameter  $\tau$ , often and in our case chosen to be 0.5 (Twigg 2003). The higher degree of the cubic polynomial makes the interpolated field lines smoother and the extreme values do not have to be at the grid points anymore as illustrated in Fig. 3b. The divergence is also not conserved by this approach but expected to be smaller than in the case of TL due to the higher order of the polynomial.

It is also possible to interpolate on the grid data with less information than in the case of TL, like in the case of the *nearest neighbor* interpolation, hereafter abbreviated as NN. Hereby, the data from the closest grid point with respect to the current spatial position is chosen without taking any additional grid points into account (see Fig. 3c). This routine is the less computational intense. While also not divergence conservative, it still preserves physical constraints as the root-mean-squared field strength, provided at the grid points. Moreover, there are none of the previously discussed issues with respect to treatment of vectorial data.

With respect to the huge uncertainties of the Galactic and extragalactic magnetic field structure, the error by the interpolation method is most likely negligible. However, it is crucial to quantify these errors, that are in principle avoidable, and elaborate the most efficient routine taking also the computational time into account. When it comes to significant deflections by the magnetic field in the so-called diffusion regime, the particle distribution is commonly used to infer the diffusion coefficient. Especially, for such an analysis it is crucial to understand the impact of interpolated magnetic field structures on the outcome.

This work is carried out using the publicly available code CRPropa3 (Alves Batista et al. 2016), which has been extended in this work by the different interpolation routines discussed above, as well as a continuous (grid-less) turbulent magnetic field structure, as introduced in Sect. 2.2. This paper is organized as follows: In Sect. 2 the characteristics of turbulent magnetic field structures and diffusive CR propagation are summarized briefly. In addition, we introduce a method to provide a continuous (grid-less) turbulent magnetic field structure, whose performance has been optimized and compared to the grid-based routines. Afterwards, in Sect. 3 the impact of different interpolation routines on the magnetic field properties and the diffusive behavior of CRs are exposed, showing the benefits of the different routines.

## TURBULENT MAGNETIC FIELDS AND DIFFUSION

The question of the generation and maintenance of large-scale magnetic fields in the Universe is still highly debated and unsolved. The existence of intergalactic, turbulent magnetic fields has two evolutionary scenarios: Either, they

result from the evolution of primordial fields under the influence of structure formation or, they are generated by the galactic outflow of magnetic fields by winds (e.g. Kronberg (1994); Grasso & Rubinstein (2001); Kulsrud & Zweibel (2008)). Both the supercluster medium and the large-scale structures of our Universe are hardly constrained by observations. The two different scenarios may cause huge differences with respect to the magnetic field strength (Hackstein et al. 2018). Currently, only upper limits of about a few nG constrains the field strength in the voids (Pshirkov et al. 2016; Ade, P. A. R. et al. 2016). Stronger constraints can in principle be derived from the observation of gamma-ray induced cascades (Neronov et al. 2013) - it is not clear, however, how large the influence of the pair instability during the propagation of the electron-positron pairs are not well-quantified at this point (Broderick et al. 2012).

In the following, we suppose for simplicity that a uniform isotropic turbulent magnetic field is present within these large-scale structures and consider the propagation of individual CRs through these fields. The field will be characterized as follows:

- (i) the root mean squared strength  $B_{\text{rms}} = \sqrt{\langle B^2(x) \rangle}$ ; and
- (ii) the distribution of magnetic energy  $w$ , which is usually given by a power-law in Fourier space, i.e.

$$w(k) = \frac{B_{\text{rms}}^2}{8\pi} k^{-m} \frac{(m-1) k_{\text{min}}^{m-1}}{1 - (k_{\text{max}}/k_{\text{min}})^{m-1}}, \quad (3)$$

between a minimum and maximum wave-number,  $k_{\text{min}}$  and  $k_{\text{max}}$ , respectively.

In the following a Kolmogorov spectrum of turbulence with  $m = 5/3$  will be considered, where the initial energy is injected at a maximum scale  $l_{\text{max}} = 2\pi/k_{\text{min}}$ . Here, it is transferred by wave interactions to lower scales until it dissipates at  $l_{\text{min}} = 2\pi/k_{\text{max}}$ . Further, the characteristic scale on which the magnetic field will vary, the so-called coherence length  $l_c$  is given in the case of uniform isotropic turbulence by (e.g. Harari et al. (2014))

$$l_c = \frac{8\pi^2}{B_{\text{rms}}^2} \int_0^\infty \frac{dk}{k} w(k) = \frac{l_{\text{max}}}{2} \frac{m-1}{m} \frac{1 - (l_{\text{min}}/l_{\text{max}})^m}{1 - (l_{\text{min}}/l_{\text{max}})^{m-1}} \simeq \frac{l_{\text{max}}}{5}, \quad (4)$$

where the latter uses  $l_{\text{min}} \ll l_{\text{max}}$  and Kolmogorov turbulence. An efficient interaction with the magnetic wavemodes only happens, if the Larmor radius  $R_L = E/(Ze B_{\text{rms}})$  of the CR with an energy  $E$  and charge  $Ze$  is smaller than the coherence length. Hence, the dimensionless rigidity  $\rho = R_L/l_c$  is the crucial quantity of the CR particle with respect to its interaction with the magnetic field.

The particles undergo resonant scattering with the turbulent wavemodes for a pitch-angle cosine  $\mu$  that satisfies  $\mu k = 1/R_L$ . Thus,  $k_{\text{min}} \leq 1/R_L$  leads to the critical rigidity  $\rho = 1$ , which divides the resonant regime at low rigidities from the quasi-ballistic regime at high rigidities. So, at  $\rho \gg 1$  the CRs propagate quasi-rectilinear providing deflections after traversing a distance  $l_c$  of the order  $\sim l_c/R_L$ . Further, the resonant scattering with the turbulent wave modes is only possible in case  $k_{\text{max}} > 1/R_L$  leading to the minimal rigidity criterion  $\rho \gtrsim l_{\text{min}}/l_{\text{max}}$ . Hence, the impact of the interpolation routine is most likely the strongest at the resonant regime at  $l_{\text{min}}/l_{\text{max}} \lesssim \rho \lesssim 1$ , where diffusive particle propagation takes place. So, the characteristic quantity is given by the diffusion coefficient, which determines the spatial distribution of the particles. But in order to obtain the impact of interpolated turbulent magnetic field structures on this quantity, a proper magnetic field structure at every point in space is needed. Note that especially at small rigidities ( $\rho \ll 1$ ) the particle transport is also effected by field line random walk, where the particle follow the magnetic field lines that diffuse in space (e.g. Subedi et al. (2017); Jokipii & Parker (1968)).

### Diffusive Transport

This section introduces the diffusion coefficient and establishes the relationship with the simulated distribution functions so that the influence of the interpolation routine for this physical quantity can be investigated. In principle, the spatial distribution of charged particles in three-dimensional space after sufficient long propagation time is described by the diffusion equation, neglecting all influences except the isotropic turbulent magnetic field (e.g. Berezhinskii et al. (1990); Schlickeiser (2002); Shalchi (2009))

$$\frac{\partial N(x, y, z, t)}{\partial t} = \kappa_{xx} \frac{\partial^2 N(x, y, z, t)}{\partial x^2} + \kappa_{yy} \frac{\partial^2 N(x, y, z, t)}{\partial y^2} + \kappa_{zz} \frac{\partial^2 N(x, y, z, t)}{\partial z^2}, \quad (5)$$

where the spatial diffusion coefficient is defined as

$$\kappa_{ii} = \frac{v_i^2}{8} \int_{-1}^{+1} d\mu \frac{(1 - \mu^2)^2}{D_{\mu\mu}}. \quad (6)$$

Here,  $\mu$  denotes the cosine of the pitch angle,  $v_i$  is the particle velocity which is subsequently estimated by the speed of light  $c$ , and  $D_{\mu\mu}$  is the diffusion coefficient (see Shalchi (2009) for a detailed review). The mean free path  $\lambda = 3\kappa/c$  determines the time required until the diffusive propagation regime is reached and the particle distribution can be described by the diffusion equation in the limit of relativistic particle velocities. In the case of an isotropically emitting point source, i.e.  $N(x, y, z, 0) = N_0\delta(x)\delta(y)\delta(z)$ , the separation approach  $N(x, y, z, t) = \rho(t)P(x)P(y)P(z)$  leads to the particle distribution

$$N(R, t, \kappa) = \frac{N_0}{8\sqrt{\pi^3\kappa^3t^3}} \cdot \exp\left(-\frac{R^2}{4\kappa t}\right) \quad (7)$$

at time  $t$  larger than  $\lambda/c$  at a distance  $R = \sqrt{x^2 + y^2 + z^2}$ . Here, it is used that for isotropic turbulent fields, the diagonal components of the diffusion tensor are all equal, so that  $\kappa_{xx} = \kappa_{yy} = \kappa_{zz} = \kappa$ .

In the following, we propagate  $N_0 = 20,000$  particles from a single, arbitrary source position through an isotropic, homogeneous turbulent magnetic field structure and collect all particles that pass an observer sphere with a radius  $R \gg \lambda$ , that is centered at the source position. Hereby, the particles can repeatedly pass through the observer surface and the collected particles were divided into 100 bins with an equal number of particles. The temporal evolution of particles is provided by their trajectory lengths  $d_{\text{traj}}$  according to  $t = d_{\text{traj}}/c$ . Since we can only compute the particle propagation for a finite period of time, we reject particles from the simulation in the case of a trajectory length that is about a magnitude above the mean trajectory length  $\bar{d}_{\text{traj}}$ . Thus, only a minor part of the tail of the particle distribution is missing, and the analytically expectation (7) can be fitted to the resulting particle distribution at a given distance  $R$ , so that the fit parameter provides the diffusion coefficient  $\kappa$ . This method is used for the first time for the determination of the diffusion coefficient of CRs. In previous investigations (e.g. Snodin et al. (2016); Subedi et al. (2017)) of the diffusion coefficients the Taylor-Green-Kubo formalism (Kubo (1957); Shalchi (2009)) method is applied, where the diffusion coefficient is given by  $\kappa_{ii} = \lim_{t \rightarrow \infty} \langle (x_i(t) - x(0))^2 \rangle / t$  after the particles entering the diffusive propagation phase.

### *Turbulent magnetic fields without interpolation*

#### *Procedure*

In general, interpolation appears to be unavoidable when running simulations on grid-based magnetic fields. However, when the grid is derived from a mathematical procedure, the grid is not necessarily needed as the procedure itself provides the field at any point in space.

According to Sect. 2, Kolmogorov-type turbulence is defined by a power-law distribution of wavemodes in the so-called k-space. Technically speaking, the grid-based turbulent magnetic fields are usually generated with the help of an Inverse Fast Fourier Transform (IFFT): A grid in k-space is populated with values according to the given power-law behavior (3); then, an IFFT is used to obtain the corresponding grid in x-space, which provides the turbulent magnetic field.

However, in a method pioneered by Giacalone & Jokipii (1999) and improved on by Tautz & Dosch (2013), hereafter referred to as TD13, the grid is eliminated completely. During setup, the wavemodes are generated in a way similar to the grid-based method, except that (a) the wavemodes are not confined to any grid, and (b) in most cases, significantly less wavemodes are used. At this stage, no field generation in x-space actually occurs.

Instead, when the value of the field is requested at a particular location in space, all of the pre-generated wavemodes are evaluated at that point in space, then added together. This procedure would be mathematically equivalent to the action of an IFFT when evaluated using grids in k- and x-space, ignoring constant factors<sup>2</sup>.

As part of this work, the TD13 method has been implemented in CRPropa following the description in Tautz & Dosch (2013), except for two differences, as follows:

<sup>2</sup> Though in practice, with this method, grids are neither used in k- nor x-space. Evaluating the typically large number of wavemodes of a k-space grid — similar to an IFFT — would not be tractable in terms of run-time: Consider that the IFFT only needs to be performed once, at setup, while this method must run each time the magnetic field is queried.

First, the current implementation uses a straight power-law in  $k$ -space, instead of the broken power-law suggested by Tautz & Dosch (2013). As described there, we could also get rid of the normalization factor due to the built-in normalization procedure. Lastly, since the  $k$  are logarithmically spaced,  $\Delta k \propto k$ . The  $\Delta k$  is part of the normalization, so the constant factor can be ignored. Thus, our implementation uses

$$A^2(k_n) = G(k_n)k_n \left( \sum_{\nu=1}^{n_m} G(k_\nu)k_\nu \right) \quad (8)$$

where  $n_m$  denotes the number of wavemodes and  $G(k) = k^{-m}$  with the spectral index  $m$  of the turbulence spectrum.

Second, TD13 normalize the field to  $B_{\text{rms}} = 1$  (unitless). To obtain a field that reproduces a certain  $B_{\text{rms}}$ , we simply multiply the desired  $B_{\text{rms}}$  onto the normalized formula.

In total, the continuous isotropic turbulent magnetic field in  $x$ -space is given by

$$\vec{B}(\vec{x}) = \sqrt{2}B_{\text{rms}} \sum_{n=1}^{n_m} \xi_n A(k_n) \cos(\vec{k}_n \cdot \vec{x} + \beta_n) \quad (9)$$

where  $\vec{k}_n = k_n \vec{\kappa}_n$ ,  $\beta_n = \zeta_n$ ; and  $\vec{\kappa}_n$ ,  $\xi_n$ , and  $\zeta_n$  are generated according to the process described by TD13.

A visual representation of the resulting field is shown in Fig. 3d.

#### Number of wavemodes

In principle, the previously given algorithm (9) allows an exact calculation of the magnetic field at any position in  $x$ -space only in the case of  $n_m \rightarrow \infty$ . However, a huge number of wavemodes makes the algorithm computationally intense and therefore difficult to use for CR propagation. Hence, we first need to determine the sufficient number of wavemodes in order to obtain a certain precision. A one to one comparison of the resulting turbulent magnetic fields for different  $n_m$  is only possible with respect to their influence on CR propagation. In the left Fig. 1, we show the distribution of particles dependent on their trajectory length, that results from the simulation of particle emission by a point source in the previously described turbulent magnetic field using a different number of wavemodes. We use the expectation (7) from diffuse transport and determine the diffusion coefficient  $\kappa$  dependent on  $n_m$ . The fit results as well as the  $3\sigma$  confidence interval are shown by the colored lines and bands, respectively. The case of  $n_m = 1200$  provides the reference values

$$\kappa_{1200} = \begin{cases} (1.536 \pm 0.011) \cdot 10^{35} \text{cm}^2/\text{s} & \text{for } l_{\text{min}}/l_{\text{max}} = 0.0046 \\ (1.512 \pm 0.010) \cdot 10^{35} \text{cm}^2/\text{s} & \text{for } l_{\text{min}}/l_{\text{max}} = 0.0167 \\ (1.466 \pm 0.010) \cdot 10^{35} \text{cm}^2/\text{s} & \text{for } l_{\text{min}}/l_{\text{max}} = 0.0971 \end{cases} \quad (10)$$

for  $\rho = 1$  that are subsequently used to determine the error  $\text{err}(\kappa)$  for a smaller number of wavemodes as shown in the right Fig. 1. In the case of a small number of wavemodes ( $n_m < 40$ ) the right Fig. 1 shows a significant impact by the width of the turbulent spectrum in  $k$ -space, i.e. the ratio of  $l_{\text{min}}/l_{\text{max}}$ . So, the error decreases for an increasing  $l_{\text{min}}/l_{\text{max}}$ , which refers to an increasing wavemode density. Hence, the resonant scattering for a narrow regime is better described leading to a smaller  $\text{err}(\kappa)$ . In the case of  $n_m \geq 40$ , the resulting uncertainty on the diffusion coefficient stays below 5% and reaches about the order of the statistical uncertainties at about 100 wavemodes. However,  $\text{err}(\kappa)$  converges faster in the case of a smaller ratio of  $l_{\text{min}}/l_{\text{max}}$ . Note that even in the case of  $n_m \gg 100$  the resulting  $\kappa$  shows minor differences dependent on  $l_{\text{min}}/l_{\text{max}}$ , although we kept  $l_c$  constant. Since this influence is not expected from the resonant scattering regime, we suppose that this is a consequence of another transport effect like the field line random walk. However, further investigations on this issue are needed but beyond the scope of this work.

#### Optimization

Since the time needed to evaluate eq. 9 roughly scales linear with the number of wavemodes, physical accuracy – requiring more wavemodes – and optimization of runtime – requiring fewer wavemodes – can be traded off against each other. However, an important consideration is the constant factor in this relation, in other words, the amount of time needed per wavemode. Lowering this amount of time would ease the trade-off described above, by allowing more wavemodes to be computed in less time. Often, the minimal number of wavemodes is set by physical requirements; the corresponding runtime then decides the viability of the simulation.

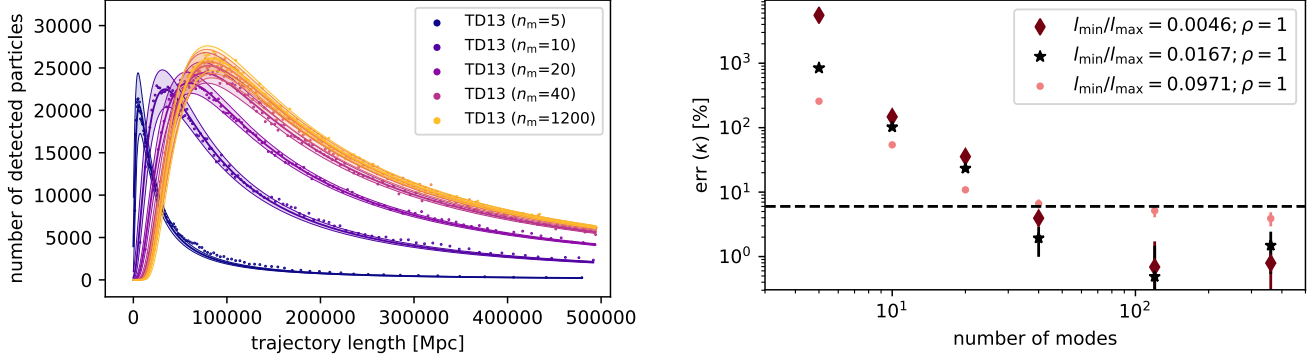


**Figure 1. Left:** Distribution of the number of particles with  $\rho = 1$  on an observer sphere with a radius of 900 Mpc using TD13 with a different number of wavemodes in the case of  $l_{\max} = 4.78$  Mpc,  $l_{\min} = 0.008$  Mpc. The function in eq. 7 is used for the fit and the error band is calculated using three sigma confidence. **Right:** The error of  $\kappa$  dependent on the number of wavemodes with respect to  $\kappa$  at 1200 wavemodes as given in eq. 10.

In our case, for 120 wavemodes, a straightforward implementation of eq. (9) turns out to be prohibitively slow, leading to simulations that take more than 20 times longer than the default trilinear interpolation. We have therefore developed an optimized implementation, which is now able to make up that factor of 20 and provide performance comparable to the trilinear interpolation due to three technical adjustments:

- We rewrote the implementation to use "single instruction multiple data" (or SIMD) processor instructions, which allow each processor core to process multiple numbers in parallel.
- We changed the way the wavemode data is stored: The code now does some pre-computations at setup time and prepares the data such that each wavemode can be evaluated with minimal cost.
- Lastly, building on the previous step, we sped up the evaluation of the cosine function itself. In particular, we simplified the argument reduction process (see also Muller 2006) by computing  $\cos(\pi a)$  instead of  $\cos(a)$ ; we also integrated a custom cosine implementation based on the highly optimized code from Shibata & contributors (2010 – 2019).

Since the SIMD instructions are not part of the base x86/64 instruction set, and their availability varies across different processors, we provide three different implementations:

- The non-optimized reference version, which is a straightforward implementation of the formula and is used to verify the optimized versions.
- The main optimization result, which uses AVX instructions for SIMD and optionally supports the FMA extension for a small performance boost. This configuration should be present on most modern systems.
- A backport of the AVX version to its predecessor, SSE. Since SSE only allows for simultaneous manipulation of two double-precision floats (as opposed to four in the case of AVX), this version incurs about a 2x performance penalty compared to the AVX version. However, it is still a lot faster than the reference implementation, so this is recommended for older systems which do not support AVX.

As an additional note, the AVX version should be treated with care, since it might cause the processor to slightly reduce its clock frequency, which would affect the rest of the simulation as well. In our simulations, this effect was not noticeable for large numbers of wavemodes. However, this may change if more code, such as an interaction module, runs between consecutive queries of the magnetic field. If this slowed the overall simulation down by more than a factor of two, the SSE version would become preferable, since SSE does not affect the CPU clock. Overall, this is something that should only become problematic in a few cases, especially since the AVX frequency reduction can be triggered unintentionally by other parts of the code. In these cases, a quick performance comparison should help select the optimal implementation.



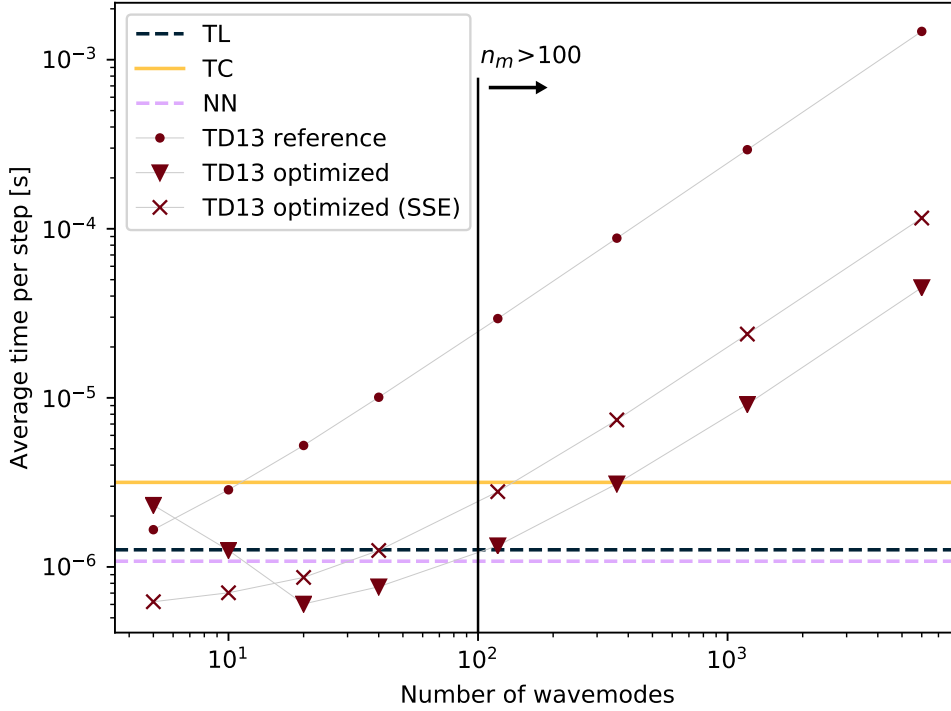


**Figure 2.** Performance of various magnetic field methods in test simulations. The grid-based methods (TL, TC, NN) do not have a parameter that affects their runtime, so they are drawn as horizontal lines. Data for TD13 is shown for different numbers of wavemodes and our recommendation for  $n_m > 100$  is indicated by the vertical line.

### Performance

To measure the performance of each method in the overall system, a simple test simulation was set up. The simulation would propagate a certain number of particles through the magnetic field using the `PropagationCK` module. To exclude unwanted side effects and achieve comparability between methods, each particle was propagated for the exact same number of simulation steps; this was achieved by setting the step size to a constant value and imposing a maximum trajectory length as a stop condition. The CPU time for each execution run was measured with Linux's `time` utility in a "best-of-3" system: Each configuration was run three times; at the end, the fastest value was taken. All simulations were performed on the same computer setup.

In order to avoid unwanted influence from setup-time operations (such as generating the grid for grid-based methods), each method was run with  $1 \times 10^4$ ,  $2 \times 10^4$ ,  $3 \times 10^4$ , and  $4 \times 10^4$  particles. Using linear regression, the slope of a fit through these points was obtained, yielding the average time per particle. This was then divided by the number of steps for each particle to obtain the average time per step, shown in Fig. 2 as a function of the number of wavemodes.

TD13 was tested on multiple counts of wavemodes, since these influence performance; the grid-based methods do not depend on a parameter that affect their runtime, so they are shown as horizontal lines.

With respect to the different interpolation routines the computational time increases with increasing interpolation effort, so that TC takes about three times longer than NN. The grid-less TD13 field shows the longest computation time in the case of the non-optimized algorithm for  $n_m > 10$ . In the case of the recommended number of wavemodes of  $n_m > 100$ , the routine is already ten times slower than TC, hence hardly feasible for the propagation of a sufficient number of particles. However, with the previously introduced optimization, the computation time can be reduced by more than an order of magnitude for  $n_m \gtrsim 20$ . Thus, the performance of the most-optimized TD13 algorithm for 100 wavemodes equals the one of TL, so that there is in principle no benefit in restricting the simulations to grid-based turbulence fields.

## THE INTERPOLATION ERROR

In the following a typical turbulent extragalactic magnetic field setup with  $B_{\text{rms}} = 1 \text{ nG}$  and  $l_c \simeq 1 \text{ Mpc}$  is used to compare the different concepts to interpolate the magnetic field strength and determine the interpolation error with respect to the reference field (TD13). Figure 3 shows a qualitative overview of the different concepts of the interpolation methods (a: TL; b: TC; c: NN and d: TD13). Clearly, Fig. 3a-c show the same underlying structure defined by the field parameters. However, it can be seen that TL produces an artificial grid-like structure, due to an a priori higher field strength at the gridpoints. These artifacts are smoothed out using TC, since the eq. 2 can even provide an interpolated value that exceeds the values that are given at the grid points. As expected, NN produces a blocky image, where the edge length of each cell expresses the used spacing  $d$  of the grid, since the same nearest neighbor value is used within a volume of  $d^3$ . TD13 is not exactly comparable due to its statistical nature. However, a qualitatively comparable sliceplot is shown in 3d.

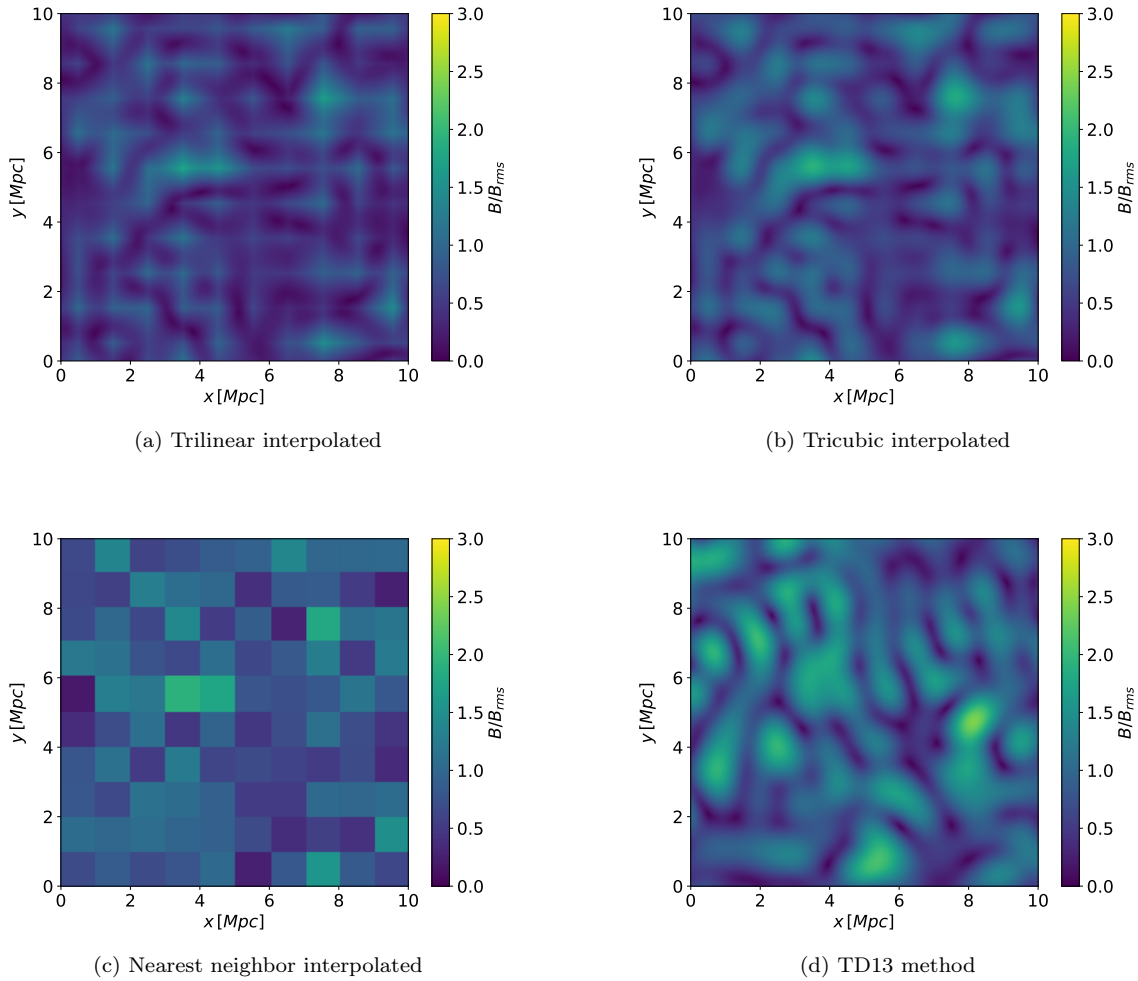


**Figure 3.** Sliceplots (at  $z=64 \text{ Mpc}$ ) showing an extract of the same turbulent field interpolated with the three different methods TL, TC, NN and a comparable field generated with the TD13 method in the case of a coherence length of 1 Mpc. The color represents the magnetic field strength normalized by the root-mean-squared strength.

In the following a quantitative comparison of the different interpolation routines is made, where we vary the magnetic field parameters  $l_{\text{min}}$ ,  $l_{\text{max}}$  as well as the sampling resolution  $l_{\text{min}}/d$  of the magnetic field saved on the grid structure, but keep  $B_{\text{rms}}$  and  $l_c$  fixed. Moreover, we keep the simulation volume  $(Nd)^3$  spanned by the grid constant (though periodically repeated if needed). In doing so, we ensure that the main characteristics of the turbulent magnetic field in



the x-space has not changed and hence, keep the diffusion coefficient fixed, as it depends on  $l_c$  but not on  $l_{\min}$  or  $l_{\max}$ . In addition, the available memory (we used roughly 8 GB for the grid storage and another 10 GB for the turbulence generation during its runtime) and the sampling theorem, which implicates that

$$l_{\min} \geq 2d \quad \text{and} \quad l_{\max} \leq nd/2, \quad (11)$$

give further constraints on the realization of different sampling resolutions as well as the ratio of  $l_{\min}/l_{\max}$ . So, we realize six different cases — the limiting cases as well as two intermediate ones — using three different sampling resolutions and three different  $l_{\min}/l_{\max}$  ratios. The impact of the interpolation routine will expose the strongest for a small value of  $l_{\min}/d$  and  $\rho \sim l_{\min}/l_{\max}$ . The CR rigidity is varied between  $\rho = 0.01$  and  $\rho = 1$  within the resonant scattering regime. In principle, a vanishing wave interaction to lower scales leads to  $l_{\min}/l_{\max} \sim 1$ . For such an extreme scenario, the resulting particle distribution is heavily affected by the interpolation routine (as shown in Fig. 4) yielding differences of the corresponding diffusion coefficient of more than 100%. With respect to the expected distribution given by TD13, the NN method provides the smallest and the TL method the largest propagation errors. However, we are not aware of any astrophysical situation where such a narrow wave spectrum is realized and keep  $l_{\max}$  at least a magnitude above  $l_{\min}$ .

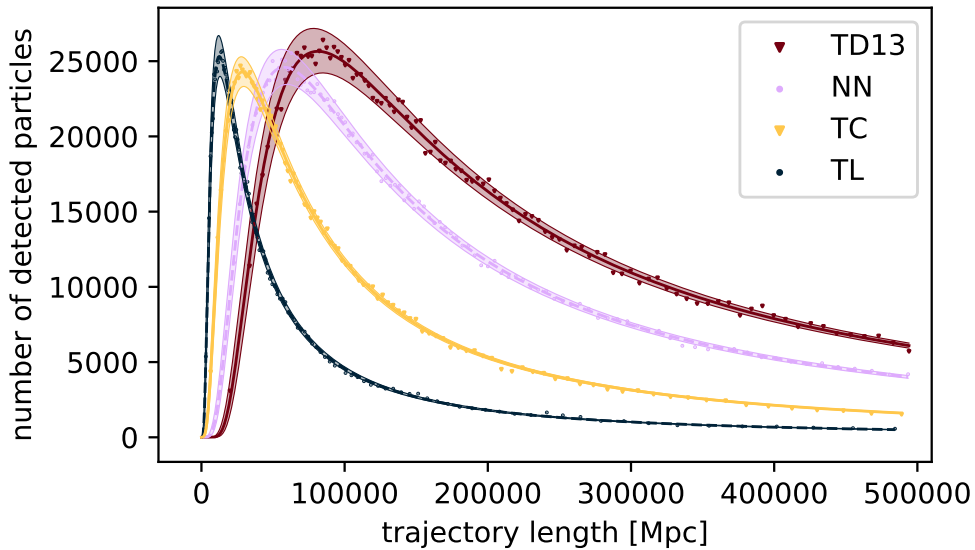


**Figure 4.** Distribution of the number of particles with  $\rho = 1$  on a sphere with  $R = 900$  Mpc dependent on the particle's trajectory length for an extreme case where  $l_{\min}/d = 2$  and  $l_{\max}/l_{\min} = 1.045$ . The function in eq. 7 is used for the fit and the error band is calculated using three sigma confidence.

### Magnetic field properties

First, we compare the root mean squared field strength  $B_{\text{rms}}$  that we obtain from the magnetic field strength  $B(x)$  at arbitrary spatial positions dependent on the interpolation routine with reference to the exact value of  $B_{\text{rms}} = 1$  nG initially given to create the fields. We pick  $10^7$  samples and, to estimate the size of statistical uncertainties, split the data set in ten parts. We calculate the  $B_{\text{rms}}$  for the different routines for each set individually in order to use the mean and its standard deviation as the basis to calculate the deviation and its error itself through Gaussian error propagation (the latter one will turn out being too small to be visible in the plot). Figure 5 shows the error in  $B_{\text{rms}}$  as a function of  $l_{\min}/d$  for three different ratios of  $l_{\min}/l_{\max}$ . The interpolation routines TC (left panel) and TL (right panel) cause an error in the reproduction of the  $B_{\text{rms}}$  which is limited to below 10%. It is the largest for small values of  $l_{\min}/d$ , increases with larger ratios  $l_{\min}/l_{\max}$  and is generally larger for the TL method as compared to the TC approach. For fundamental reasons, NN does not yield any deviations except for the statistical uncertainties, so that it is not illustrated.

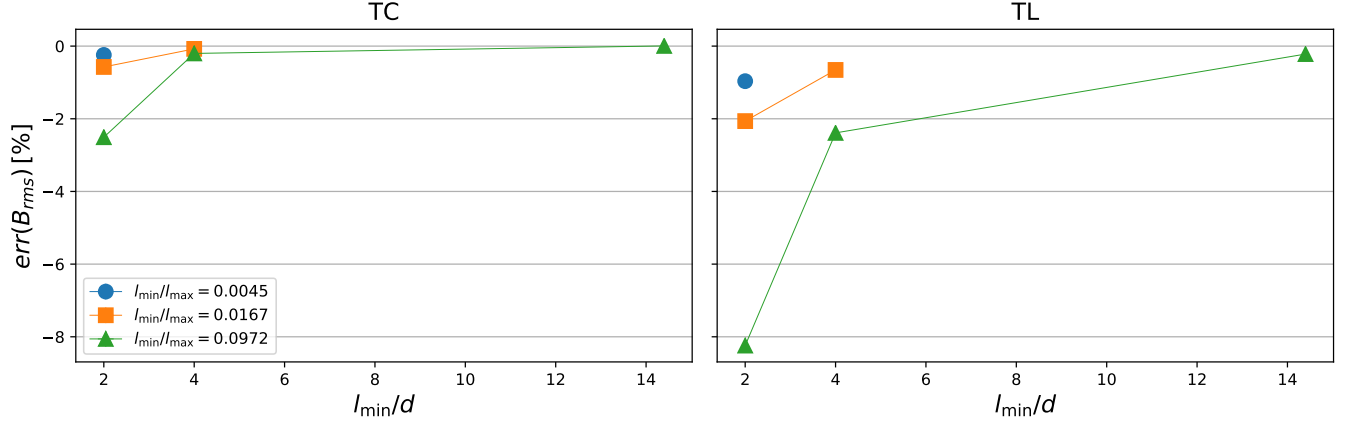


**Figure 5.** Relative deviation of the  $B_{rms}$  in comparison to the initially given 1 nG for different  $l_{\min}/l_{\max}$  ratios and samplings (as far as the setup allowed it to have data points) for the interpolations TL and TC, using  $10^7$  randomly drawn values each plotted data point.

In total, the impact of the interpolation routine is negligible for  $l_{\min}/d \gg 1$  or  $l_{\min}/l_{\max} \ll 1$ .

Secondly, we would like to obtain a measure of the B-field divergence in each method. Straight-forward differentiation, however, is not possible: TL is not differentiable, and NN is not even continuous. For this reason, we instead use the Gauss Theorem and compute the net flux through small regions of space, defined by the grid cells. The expected net flux through any region of space is always zero ( $\text{div} B = 0$ ), so that any additional or missing flux represents a flux defect. Since each interpolation method actually defines a representable function (dependent on the grid values, of course, but still a function), the surface flux integration can be done analytically. And since the method is analytical, TD13 is guaranteed to have no divergence (by construction), so it was not evaluated.

Since the actual net flux through each grid cell depends on the size of that cell's surface (which can be varied at will), it does not represent a good measure for interpolation performance. Hence, we divide out the surface area to obtain the density of the flux defect. Hence, this measure becomes independent of the grid size and only depends on intrinsic properties of the underlying system. As the distributions are all centered around zero (see Fig. 6), using the standard deviation  $\sigma_B$  of the flux distribution seems like the most sensible single-parameter measure of this quantities.

As shown in Fig. 7 all methods perform worse on more coarse-grained grids (small  $l_{\min}/d$ ) and for a small wavemode range. In all cases, TC incurs a lower flux defect than both NN and TL, while NN outperforms TL without exception. Naturally, the gap between the methods shrinks as the flux defects get smaller; for changes in  $l_{\min}/l_{\max}$ , the relative difference remains constant.

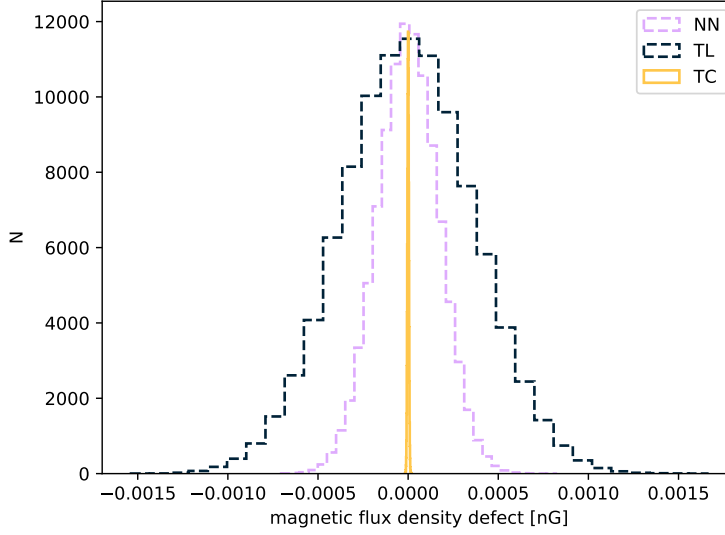


**Figure 6.** Flux defect density distribution for  $10^6$  randomly drawn grid cubes using  $l_{\min}/l_{\max} = 0.0972$  and  $l_{\min}/d = 14.4$ .

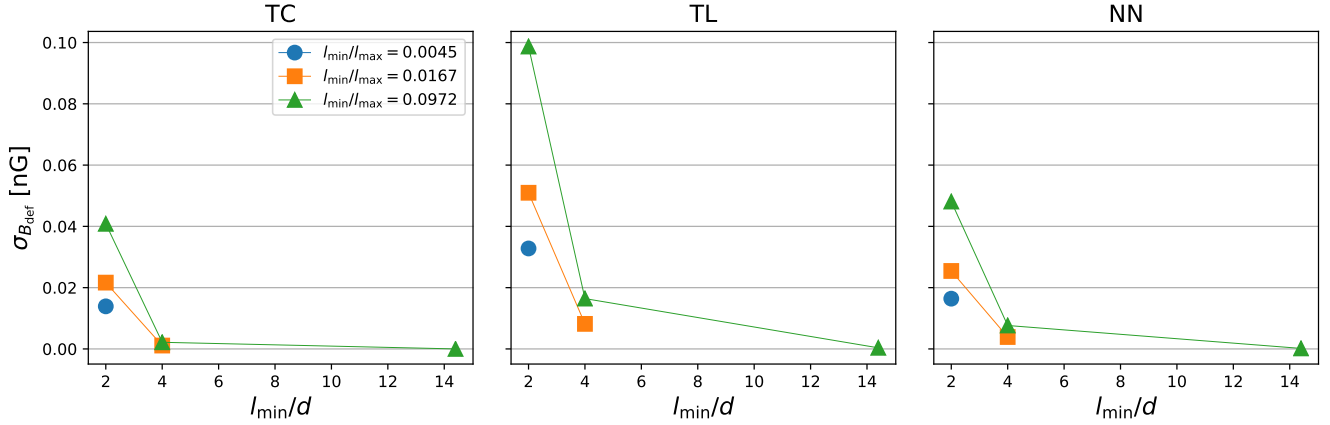


**Figure 7.** Comparison plots showing the standard deviation of the flux defect density distribution for each of the six different simulation cases and interpolation methods, using  $10^6$  randomly drawn samples each. Since the distributions are centered around zero, taking the standard deviation seems more sensible than using the mean; lower values here thus correspond to a more divergence-free field overall. Different values for  $l_{\min}/d$  are graphed along the x axis, whereas different values for  $l_{\max}/l_{\min}$  are represented by separate curves.

#### Turbulence spectrum

In addition to the interpolation effects in x-space, also the underlying wave spectrum is changed by interpolation. To analyze the wave spectrum for a given volume of space, we determine the magnetic field on some equidistant points in space that are located in the middle of cubes defined by grid points and use a fast Fourier transform (FFT) to obtain the field into  $k$ -space. Figure 8 shows the resulting weighted power-law distribution between the given minimal and maximal wave number. Due to the discretization and windowing of the continuous TD13 field by the FFT, this routine provides a non-vanishing amplitude at  $k > k_{\max}$  which, however, vanishes for an exact Fourier transform, i.e. an infinite number of transformation points. In addition, the limited number of wavemodes leads to an additional fluctuation resulting in a deviation from the desired amplitude  $A(k)$ . With respect to the interpolation routines, NN provides a priori the correct spectral behavior for the used method of analysis. In contrast, TC and especially TL have a significant impact on the spectral behavior, causing a steepening of the slope toward higher wave numbers. This

change of slope reduces the number of wavemodes the particles are able to scatter off. In particular, for a rigidity  $\rho \sim l_{\min}/l_{\max}$ , i.e. close to the limit of the resonant scattering regime, the diffusive behavior is expect to change due to the steeper spectral slope by the interpolation routine, as analyzed in more detail in the following section.

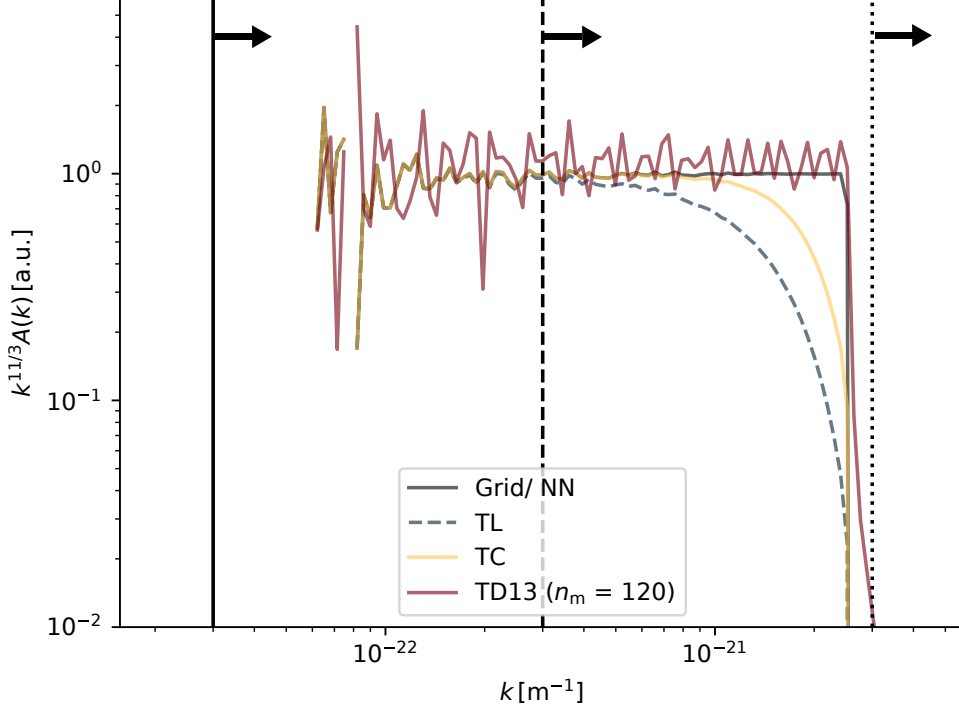


**Figure 8.** Spectrum of the turbulent magnetic field in k-space in the case of  $l_{\min}/l_{\max} = 0.017$ . **Grid**: sampled on gridpoints, **TL**: trilinear interpolated, **TC**: tricubic interpolated, **TD13**: TD13 method with 120 wavemodes. The vertical lines mark the lower rigidity bound for the resonant scattering of particles with  $\rho = 1$  (solid line),  $\rho = 0.1$  (dashed line) and  $\rho = 0.01$  (dotted line).

### The Diffusion Coefficient

The mean of the reference values of the diffusion coefficient according to eq. 10 yields a mean free path  $\lambda \lesssim 5$  Mpc in the case of  $\rho \lesssim 1$ , since  $\lambda$  decreases with decreasing rigidity. Hence, the number of CR particles with  $l_{\min}/l_{\max} \lesssim \rho \lesssim 1$  at a given distance  $R \gg 5$  Mpc dependent on the trajectory length  $ct$  enables us to determine the diffusion coefficient  $\kappa$ . Note that due to the diffusive behavior of the CR particles at  $R \gg 5$  Mpc,  $\kappa$  is independent of the spherical observer radius  $R$ .<sup>3</sup> So, the analytical expression (7) for the expected number of the particles as a function of time on the spherical observer with radius  $R$  is used to determine  $\kappa$ . Simulations with TD13 using 1200 wavemodes provide the reference values of the diffusion coefficient. Figure 9 shows the percental error of the diffusion coefficient as a function of  $l_{\min}/d$  for three different ratios  $l_{\min}/l_{\max}$ . The three panels show the results for TC (left), TL (middle) and NN (right) methods. It can be seen that, once again, TL results in the largest interpolation error, in particular in the case of a low grid resolution ( $l_{\min}/d = 2$ ) and a small ratio  $l_{\min}/l_{\max} \simeq \rho$  yielding  $\text{err}(\kappa) = |\kappa_{\text{TD13}} - \kappa_{\text{TL}}|/\kappa_{\text{TD13}} \simeq 0.13$ . However, at a two times higher grid resolution or a six times smaller  $l_{\min}/l_{\max}$  ratio the relative error already decreases significantly to a few percentages. Still, the other interpolation routines provide significantly lower errors with respect to  $\kappa$ , in particular TC. It surprises at first that an increasing grid resolution does not decrease the interpolation error, and  $\text{err}(\kappa)$  even increases significantly in the case of NN. In the latter case, an increasing grid resolution also

<sup>3</sup> However, in the case of sub- or super-diffusion this is no longer valid and  $\kappa = \kappa(R)$ .

increases the number of discontinuous changes of the magnetic field, which distorts the field line random walk that starts dominating the transport at  $\rho \lesssim l_{\min}/l_{\max}$ . So, for  $\rho < l_{\min}/l_{\max}$  and  $l_{\min}/d = 2$ , the particle's Larmor radius

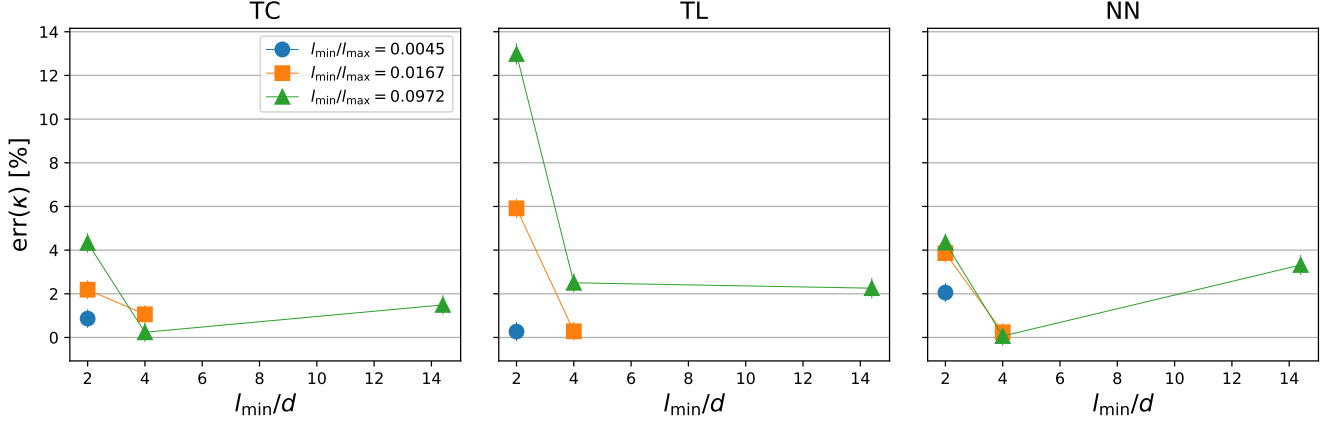


**Figure 9.** Six different simulation cases are used to present the error in the calculation of the diffusion coefficients for different interpolation routines using particles with  $\rho = 0.1$ . Each case is a fixed combination of the ratios  $l_{\min}/d$  and  $l_{\min}/l_{\max}$  (as far as the setup allowed it to have data points) within the resonant scattering regime.

is smaller than the grid resolution ( $R_L < 2d/5$ ). Thus, the particle essentially follow the magnetic field line that is smoothed in the case of TL or TC and unchanged in the case of NN. But also the grid-less TD13 field does not change significantly on these length scales, as already illustrated in Fig. 3(d), since  $\rho < l_{\min}/l_{\max}$  implicates that  $R_L < l_c$ . Hence, the interpolation error most likely decreases in the rigidity regime where field line random walk dominates the particle transport. But in case of resonant scattering at small rigidities, i.e.  $1 \gg \rho > l_{\min}/l_{\max}$ , a high grid resolution is needed according to the sampling theorem (11). Due to limited memory space a grid can hardly be resolved better than a few thousand cubed grid points along each of the three coordinate axes, which exposes the need for the optimized TD13 method in the case of resonant scattering at  $\rho \ll 1$ .

In the case of  $\rho = 1$ , particles with a large pitch-angle cosine start to leave the resonant scattering regime, so that the diffusive behavior according to eq. 7 already gets distorted, due to the limited scattering regime, leading to a significantly higher uncertainty of the resulting  $\kappa$ . Therefore, the resulting  $\text{err}(\kappa)$  does not provide conclusive answers, but  $\text{err}(\kappa)$  shows in principle the same behavior as in the case of  $\rho = 0.1$ . But at  $\rho = 1$  the impact of field line random walk for the case of  $l_{\min}/l_{\max} \simeq 0.1$  is much smaller, so that a high grid resolution ( $l_{\min}/d \gg 1$ ) seems to reduce  $\text{err}(\kappa)$  even in the case of NN.

Instead of a complete analysis of all of the six previous setup cases, we consider for  $\rho = 0.01$  only the case of  $l_{\min}/d = 2$  and  $l_{\min}/l_{\max} = 4.5 \times 10^{-3}$  due to the limited available CPU time. Here, Figure 10 shows the resulting rigidity dependence of the percental error in the determination of the diffusion coefficient for the three methods in the range  $0.01 < \rho < 1$ . The diffusive behavior of the particles is predominantly disturbed for TL in the case of  $\rho \sim l_{\min}/l_{\max}$ . Hereby, only the steepened part of the turbulent spectrum (see Fig. 8) is able to interact with the particle leading to a large  $\text{err}(\kappa)$  — similar to the case of  $0.1 = \rho \sim l_{\min}/l_{\max}$ . At  $\rho \gg l_{\min}/l_{\max}$  the more accurate part of the interpolated turbulence spectrum is part of the resonant scattering regime leading to a smaller error of the diffusive behavior.

## CONCLUSIONS

Turbulent magnetic fields that provide the dominant magnetic field structure in a multitude of astrophysical environments are commonly generated by an Inverse Fast Fourier Transformation on a homogeneous, spatial grid. Due to this discretization, the magnetic field at an arbitrary spatial position requires the use of an interpolation routine. In this work, we determine the resulting error of three different interpolation routines (TL, TC and NN) with respect to the magnetic field properties. We further quantify the diffusive behavior of CRs as a function of the dimensionless rigidity in the range  $\rho = 0.01$  to  $\rho = 1$ . It is shown that only in the case of a low grid resolution ( $l_{\min}/d \lesssim 2$ ) and a rigidity close to the lower bound of the resonant scattering regime ( $l_{\min}/l_{\max} \lesssim \rho$ ) the TL interpolation changes the

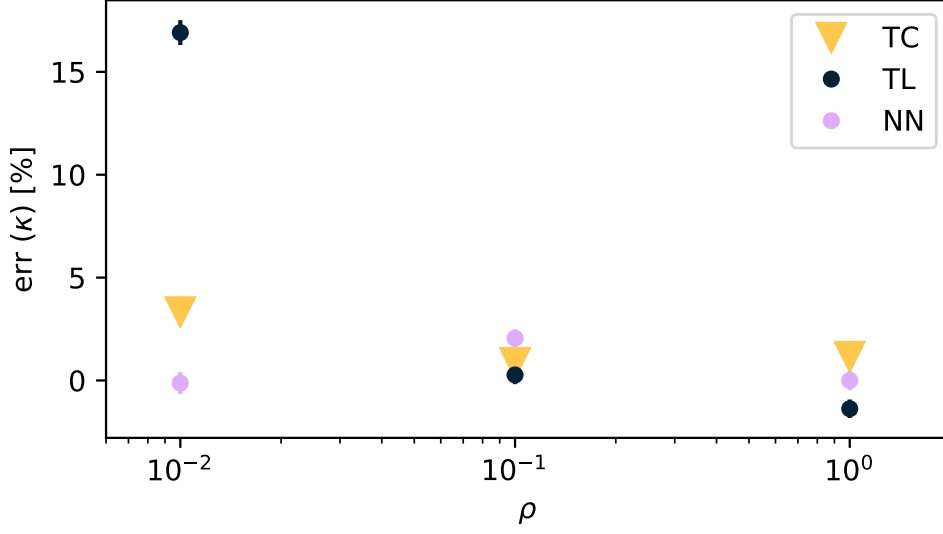


**Figure 10.** Rigidity dependence of the interpolation error of the diffusion coefficient within the resonant scattering regime. Here  $l_{\min}/d = 2$  and  $l_{\min}/l_{\max} = 4.5 \cdot 10^{-3}$  have been used.

diffusive behavior by more than 10%. Based on the significant steepening of the turbulence spectrum at  $k \sim k_{\max}$ , the resulting change of the diffusion coefficient at  $\rho \sim l_{\min}/l_{\max}$  is still quite small. But at these rigidities, the impact of the field line random walk starts dominating, so that the particles predominantly follow the local mean field and hardly scatter off the wavemodes given by the turbulence spectrum.

The other interpolation routines generate significant lower errors, in particular TC. However, since NN is significantly less CPU-intense and still very limited in its relative interpolation error, with an error on the diffusion coefficient of less than 5%, we conclude that NN is the best interpolation routine in the case of grid-based data.

In addition, we optimize the performance of a continuous grid-less method to generate isotropic turbulent magnetic fields (TD13), so that the necessary CPU time is reduced by more than an order of magnitude. Hence, in the case of 100 wavemodes, where the uncertainty of the diffusion coefficient has already decreased to a few percentages, the performance of the optimized TD13 routine is equal to TL and only the use of NN is still slightly faster. Thus, the optimized TD13 routine with about 100 wavemodes provides clear benefits compared to the grid-based approach, as the given magnetic field properties are reproduced the most accurately. In addition, the TD13 routine has also no technical difficulties — due to limited memory space — to realize the case of particles with a small rigidity within the resonant scattering regime, i.e.  $1 \gg \rho > l_{\min}/l_{\max}$ .

This work most notably benefits from the development of CRPropa3. In addition, we are grateful to Andrej Dundovic for useful discussions that helped to improve the original version of the paper. Some of the results in this paper have been derived using the software packages Numpy (van der Walt et al. 2011), Matplotlib (Hunter 2007) and its online documentation including example code, SymPy (Meurer et al. 2017), Pandas (McKinney 2010), as well as the Julia programming language (Bezanson et al. 2017). L.S., A.F. and B.E. acknowledge financial support from the MERCUR project An-2017-0009.



## REFERENCES

- Ade, P. A. R., et al. 2016, *A&A*, 594, A19
- Alves Batista, R., Shin, M.-S., Devriendt, J., Semikoz, D., & Sigl, G. 2017, *Phys. Rev.*, D96, 023010
- Alves Batista, R., et al. 2016, *JCAP*, 1605, 038
- Beck, M. C., Beck, A. M., Beck, R., et al. 2016, *Journal of Cosmology and Astroparticle Physics*, 2016, 056
- Berezinskii, V. S., Bulanov, S. V., Dogiel, V. A., & Ptuskin, V. S. 1990, *Astrophysics of cosmic rays* (North Holland)
- Bezanson, J., Edelman, A., Karpinski, S., & Shah, V. 2017, *SIAM Review*, 59, 65
- Broderick, A. E., Chang, P., & Pfrommer, C. 2012, *Astroph. J.*, 752, 22
- Giacalone, J., & Jokipii, J. R. 1999, *The Astrophysical Journal*, 520, 204
- Grasso, D., & Rubinstein, H. R. 2001, *PhR*, 348, 163
- Hackstein, S., Vazza, F., Brüggem, M., Sorce, J. G., & Gottlöber, S. 2018, *Monthly Notices of the Royal Astronomical Society*, 475, 2519
- Harari, D., Mollerach, S., & Roulet, E. 2014, *PhRvD*, 89, 123001
- Hunter, J. D. 2007, *Comput. Sci. Eng.*, 9, 90
- Jokipii, J. R., & Parker, E. N. 1968, *Phys. Rev. Lett.*, 21, 44
- Kronberg, P. P. 1994, *Reports on Progress in Physics*, 57, 325
- Kubo, R. 1957, *Journal of the Physical Society of Japan*, 12, 570
- Kulsrud, R. M., & Zweibel, E. G. 2008, *Reports on Progress in Physics*, 71, 046901
- Lekien, F., & J. E., M. 2005, *International Journal for Numerical Methods in Engineering*, 63, doi:10.1002/nme.1296
- McKinney, W. 2010, *Proc. of SciPy*, 51
- Meurer, A., Smith, C. P., Paprocki, M., et al. 2017, *PeerJ Computer Science*, 3, e103
- Müller, G. 2016, *JCAP*, 8, 025
- Muller, J.-M. 2006, *Elementary Functions* (Birkhäuser)
- Neronov, A., Taylor, A. M., Tchernin, C., & Vovk, I. 2013, *Astron. & Astroph.*, 554, A31
- Pshirkov, M. S., Tinyakov, P. G., & Urban, F. R. 2016, *Phys. Rev. Lett.*, 116, 191302
- Schlickeiser, R. 2002, *Cosmic Ray Astrophysics* (Springer)
- Shalchi, A. 2009, *Nonlinear Cosmic Ray Diffusion Theories*, Vol. 362 (Springer)
- Shibata, N., & contributors. 2010 – 2019, *SLEEF Vectorized Math Library*, GitHub
- Snodin, A. P., Shukurov, A., Sarson, G. R., Bushby, P. J., & Rodrigues, L. F. S. 2016, *Mon. Not. Roy. Astron. Soc.*, 457, 3975
- Subedi, P., Sonsrrette, W., Blasi, P., et al. 2017, *The Astrophysical Journal*, 837, 140
- Tautz, R., & Dosch, A. 2013, *Physics of Plasmas*, 20, 022302
- Twigg, C. 2003, *Catmull-Rom splines*, URL: <http://graphics.cs.cmu.edu/nsr/course/15-462/Fall04/assts/catmullRom.pdf>
- van der Walt, S., Colbert, S. C., & Varoquaux, G. 2011, *IEEE Computer Society*, arXiv:1102.1523